Available online at www.sciencedirect.com
ScienceDirect
Journal of Power Sources 175 (2008) 510–516
JOURNAL OF POWER SOURCES
www.elsevier.com/locate/jpowsour

Electrochemical performance of mesoporous TiO_2 anatase

P. Kubiak [a], J. Geserick [b], N. Hüsing [b], M. Wohlfahrt-Mehrens [a,*]

[a] *ZSW-Center for Solar Energy and Hydrogen Research, Helmholtzstraße 8, D-89081 Ulm, Germany*
[b] *Ulm University, Institute of Inorganic Chemistry I, Albert Einstein Allee 11, D-89081 Ulm, Germany*

Received 24 July 2007; received in revised form 9 September 2007; accepted 16 September 2007
Available online 21 September 2007

Abstract

Mesoporous TiO_2 was prepared via a sol–gel method from an ethylene glycol-based titanium-precursor in the presence of a non-ionic surfactant at pH 2. Only the anatase structure was detected after annealing, while the BET specific surface area was measured as being 90 $m^2\,g^{-1}$ with a rather monomodal pore diameter close to 5 nm. Electrochemical performances were investigated by cyclic voltammetry and galvanostatic techniques. Mesoporous TiO_2 exhibits excellent rate capability (184 mAh g^{-1} at *C*/5, 158 mAh g^{-1} at 2*C*, 127 mAh g^{-1} at 6*C*, and 95 mAh g^{-1} at 30*C*) and good cycling stability.

Keywords: Mesoporous materials; Anatase TiO_2; Electrochemical lithium insertion

1. Introduction

In the future, nanomaterials will become more and more important for many applications including photovoltaics, electrochemical energy storage systems, catalytic devices and sensors. Li-ion batteries are attractive power devices due to their high energy density. The successful electrochemical and chemical insertion of lithium into titanium dioxides has already been demonstrated [1,2]. TiO_2 has various polymorphs, such as anatase, rutile, brookite or TiO_2(B). The lithium insertion into these hosts has been investigated but it appears that only anatase [2–5] and TiO_2(B) [6,7] give satisfactory results. TiO_2 anatase is a promising electrode material for Li-ion batteries due to its good Li-storage capacity (335 mAh g^{-1} corresponding to the insertion of one Li per TiO_2 inducing a complete reduction $Ti^{4+} \rightarrow Ti^{3+}$), cycling stability and safety against overcharging [4]. In addition, it is a non-toxic and cheap material. From a practical viewpoint, reversible insertion of Li into anatase is about 0.6 (i.e. 200 mAh g^{-1}) at 1.78 V versus Li^+/Li [3,4]. But its electrochemical performance strongly depends on the size and shape of particles [4,8,9]. Indeed, too small particles are generally handicapped by strong charge irreversibility due to parasitic surface reactions [10]. Mesoporous materials are an interesting alternative to the micro- or nanocrystalline materials. Since Mobile discovered the M41S phases in 1992 [11], not only silica, but also mesoporous non-silica oxide, phosphates, etc., have been prepared for various applications [12–17]. Among the mesoporous transition metal oxides, crystalline porous titanium dioxide with a high surface area is a very attractive material due to its well-known activity in catalytic reactions [18]. In fact, mesoporosity is considered to be equally important in energy storage aspects, as the porosity plays an important role in the lithium insertion/extraction reactions. Few papers deal with electrochemical Li insertion into mesoporous TiO_2 anatase but some authors report unusual electrochemical properties for pure [19–22] or modified [23–25] (Al, Sn or Zr) TiO_2 anatase.

In this paper, we investigate the electrochemical performance of a mesoporous TiO_2 anatase synthesized using an ethylene glycol-modified titanium-precursor and an amphiphilic molecule as the templating agent. The glycol-modified precursor is a rather unusual precursor in sol–gel chemistry, where mostly simple alkoxides such as titanium isopropoxides are applied, but has some significant advantages, especially with respect to processing in the presence of amphiphilic surfactants [26–28]. In addition, one has to distinguish between wet chemical processing and simple thermal decomposition of the glycolate precursors as it was shown by Fröba et al. [29]. To the

* Corresponding author. Tel.: +49 731 9530 601; fax: +49 731 9530 666.
E-mail address: margret.wohlfahrt-mehrens@zsw-bw.de
(M. Wohlfahrt-Mehrens).

0378-7753/$ – see front matter © 2007 Elsevier B.V. All rights reserved.
doi:10.1016/j.jpowsour.2007.09.044

best of our knowledge the processing of EGMT in the presence of surfactants is not reported at all. We especially focused on fast deinsertion capabilities of the material prepared with this precursor.

2. Experimental

2.1. Materials

PE-*b*-PEO (Brij56, $M \sim 682\,g\,mol^{-1}$) was purchased from Aldrich. Tetraisopropylorthotitanate (TIP) (98%) as well as ethylene glycol (EG) (99.5%) was purchased from Merck and used as received. Tetrahydrofuran (THF, 99.8%) was received from Merck and distilled over sodium hydride prior to use.

2.2. Synthesis of the precursors

Bis(2-hydroxyethyl)titanate (EGMT) was synthesized by a modified procedure of Xia et al. [30] in a 1000 mL one-necked Schlenk round-bottomed flask equipped with a reflux condenser under argon. EG and TIP (molar ratio 2:1) were dissolved in THF and refluxed for 5 h at 90 °C. The isopropyl alcohol liberated and the THF were distilled off at 120 °C. EGMT was dried under reduced pressure at 170 °C and obtained as a white powder.

The resulting glycol-modified precursor was characterized by thermal analysis (TGA): EGMT (28.3 wt.% Ti). The theoretical value for Ti:glycol 1:2 is 28.5 wt.%.

2.3. Synthesis of TiO_2

In a typical synthesis 0.55 g (0.81 mmol) Brij56 was dissolved in 100 mL dilute hydrochloric acid (pH 2). To this solution 4.53 g EGMT (26.95 mmol Ti) was added and treated in an ultrasonic bath for 5 h at 60 °C. The resulting suspension was aged in an oven at 60 °C for 1 day and subsequently calcined at 400 °C for complete surfactant removal.

2.4. Structural characterization

XRD measurements were performed by using Cu Kα radiation (λ = 0.154 nm) on a PANalytical MPD PRO. SEM images were recorded on a LEO 1530 VP. Nitrogen porosimetry measurements were performed on a NOVA 4000e and Autosorp MP1 instrument (Quantachrome). The surface area was calculated according to Brunauer, Emmet and Teller (BET) in the p/p_0 range of 0.05–0.3 and the pore size distribution was determined according to Barrett, Joyner and Halenda (BJH) from the desorption branch of the isotherms.

2.5. Electrochemical evaluation

Lithium insertion/extraction property of TiO_{2meso} was investigated at room temperature by both cyclic voltammetry and galvanostatic technique using a sealed three-electrode cell equipped with metallic lithium as counter and reference electrode in a 1 M $LiPF_6$ EC/DMC (1:1, w/w) (UBE Industry; Japan). The electrode materials were prepared by mixing the active material with 12% conducting carbon black additive (Super P) and 12% PVDF binder in NMP. The well-mixed slurry was coated onto an aluminum foil using doctor blade method. The coated foil was allowed to dry in an oven at 80 °C overnight. Then circular disc electrodes were punched from the foil, uniaxially pressed for better contact of the coated material and aluminum current collector and used as cathode for assembling the tests cells. The maximum Li insertion in TiO_2 was assumed to be 0.5 ($168\,mAh\,g^{-1}$), and thus the charging rates in the measurements were based on the following relationship: $1C = 0.168\,A\,g^{-1}$. Commercial TiO_2 P25 (DEGUSSA) was used for comparison and labeled TiO_{2com}.

3. Results and discussion

3.1. Material characterization

Table 1 gives the physical properties of the studied sample. After thermal treatment at 400 °C, 4 h under air, TiO_{2meso} can be indexed as pure anatase TiO_2 (JCPDS 21-1272, $a = 3.785$ Å and $c = 9.514$ Å) without presence of other phases. The calculated cell parameters: $a = 3.785$ Å and $c = 9.514$ Å are in good agreement with the reference values. On the other hand, TiO_{2com} presents both anatase (85%) and rutile (15%) phases. The crystallite size was determined using Scherrer's equation and is about 9 nm. For comparison, the crystallite size for TiO_{2com} is 30 nm. The obtained material displays quite large agglomerates (Fig. 1) composed of almost spherical particles with a diameter of about 100 nm. Note that the presence of large agglomerates makes the electrode fabrication easier which is more difficult with nanosized materials. TiO_{2meso} presents a specific surface area of $92\,m^2\,g^{-1}$. This value is higher than the value observed for commercial TiO_2 ($48\,m^2\,g^{-1}$) but much lower than values observed for nanomaterials [5,31]. The pore size distribution was obtained using the BJH method from the adsorption isotherm (Fig. 2). For TiO_{2meso}, the isotherm can be classified as type IV according to the classification by Brunauer et al. [32]. Showing the hysteresis H2 this isotherm type is characteristic for mesoporous materials with drop-shaped pores. The sample offers a narrow pore size distribution with a maximum at 5 nm. Thus, the synthesis used in this work leads to a good control the texture (BET surface area, pore size distribution, etc.) of the material. In the follow-

Table 1
Properties of studied samples: S = BET surface area and d = crystallite size diameter from X-ray line broadening

Sample	Anatase	Rutile	Anatase/rutile (%)	S ($m^2\,g^{-1}$)	d (nm)
TiO_{2com} (P25)	$a = 3.787$ Å, $c = 9.509$ Å	$a = 4.596$ Å, $c = 2.959$ Å	85/15	48	30
TiO_{2meso}	$a = 3.785$ Å, $c = 9.514$ Å	–	100/–	92	9

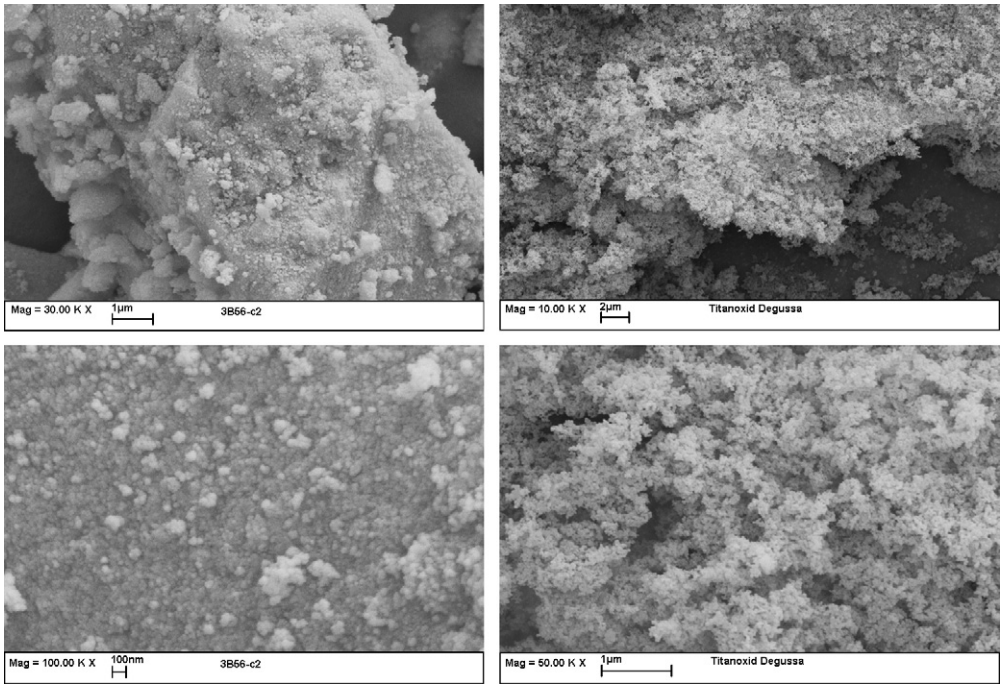

Fig. 1. SEM pictures of TiO_{2meso} (left) and TiO_{2com} (right).

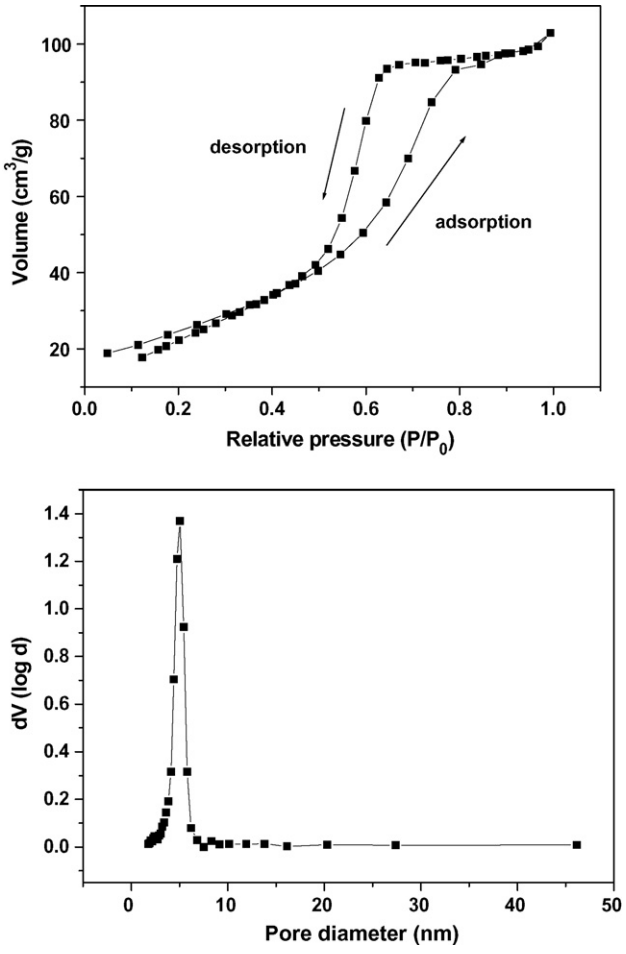

Fig. 2. N_2 adsorption–desorption isotherms of TiO_{2meso} (top) and BJH pore size distribution (bottom).

ing section, we will develop the electrochemical evaluation of this material in order to understand role of mesoporosity in the reactivity of anatase titania versus Li.

3.2. Electrochemical evaluation

3.2.1. Cyclic voltammetry

Fig. 3 shows the comparison between the voltammograms of TiO_{2com} and TiO_{2meso} anatase in 1 M $LIPF_6$ EC/DMC (1/1, w/w) at a scan rate of 0.1 mV s^{-1} for the first and second cycles. Anatase and rutile phases present in TiO_{2com} can be also detected by cyclic voltammetry. For the first cycle, cathodic/anodic peaks at ~1.7 and 2.0 V and cathodic peaks at about 1.4 and 1.0 V versus Li/Li^+ have been observed. These latter peaks have not been observed in the second cycle and can be ascribed to the rutile phase which is highly irreversible versus Li insertion/extraction. The peaks at 1.7 and 2.0 V are usually observed for polycrystalline [33] and single crystal anatase [34]. They correspond to the insertion or extraction of lithium according to the following equation:

$$TiO_2 + x(Li^+ + e^-) = Li_xTiO_2 \quad (1)$$

This reaction has been extensively studied both theoretically and experimentally [33–38]. The mechanism of Li insertion into anatase is the phase transition from tetragonal TiO_2 (space group $I4_1/amd$) to orthorhombic $Li_{0.5}TiO_2$ (space group *Imma*). It occurs a spontaneous phase separation into lithium-poor $Li_{0.01}TiO_2$ and lithium-rich $Li_{0.5}TiO_2$, and this process is characterized by a constant voltage (ca. 1.75 and 2.0 V for the insertion and extraction processes, respectively, as shown in Fig. 3). The maximum insertion capacity x of 0.5 mol of Li per 1 mol of anatase is given by the number of vacant 4b sites for Li

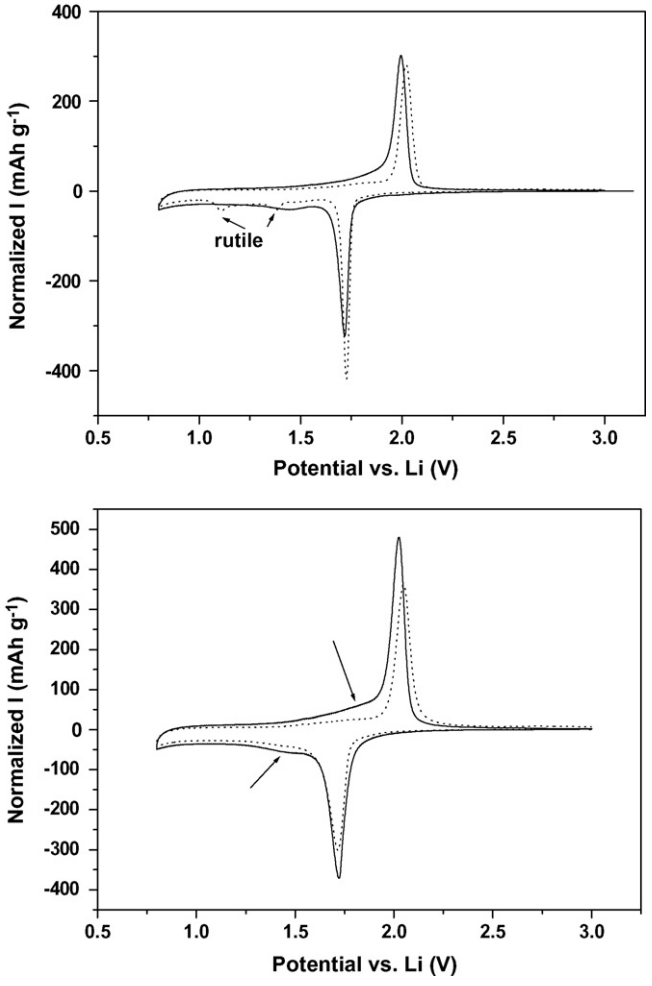

Fig. 3. Cyclic voltammetry for TiO_{2com} (dot line) and TiO_{2meso} in 1 M $LIPF_6$ EC/DMC (1/1, w/w), scan rate 0.1 mV s^{-1}: first cycle (top) and second cycle (bottom).

ions, corresponding to one-half of interstitial sites in the anatase structure [35–38].

TiO_{2meso} exhibits two oxidation/reduction pairs of peaks. One is the traditional insertion/extraction of Li^+ in Li_xTiO_2, the other are very broad and located around 1.5 V (insertion) and 1.9 V (extraction). This kind of extra feature has already been reported for mesoporous [9], nanosheets [39] or nanorods [40] TiO_2. The intensity of the extra peaks decreases as the temperature while thermal treatment is increasing. In our case the peaks are present but few intense indicating the mesoporous nature of the material. Although the exact mechanism is still unknown, it is attributed to surface storage of lithium or presence of amorphous TiO_2 inside the material.

3.2.2. Cycling abilities

Besides the main process of the two-phase Li insertion into the tetragonal phase, an additional insertion process takes place at insertion depths exceeding that of anatase. For the completely crystalline phase, this process is attributed to the further topotactic Li insertion into the Li-rich orthorhombic $Li_{0.5}TiO_2$ phase [38] or to the contributions of amorphous or disordered crystalline phases [41]. Although, the further insertion process is

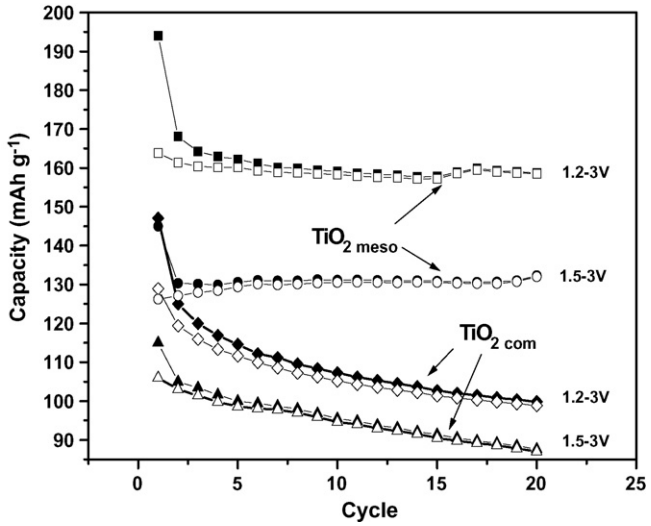

Fig. 4. Evolution of charge/discharge capacity at 2*C* rate for TiO_{2com} and TiO_{2meso}. Solid symbols are for discharge and open symbols for charge.

not characterized by any clearly distinguishable individual peaks on voltammograms, it has high insertion capacity and is highly irreversible due to repulsive interactions between inserted Li and consequent strains in the lattice [42,43]. A solution to avoid the second mechanism is to limit the potential cut-off at the end of the discharge. In this study, we have used two potential ranges: 1.2–3 and 1.5–3 V. The cycling stability under repetitive insertion/extraction at the 2*C* rate (0.335 A g^{-1}) has been investigated. 1 C corresponds to a complete charge of the electrode within 1 h. The charging/discharging capacity evolution of TiO_{2com} and TiO_{2meso} is given in Fig. 4. TiO_{2meso} shows higher capacities than TiO_{2com} for both potential windows. Moreover, the mesoporous material presents better stability. Indeed, a rapid capacity fading (80% capacity retention after 20 cycles) is observed for TiO_{2com} which is not observed for the mesoporous one. Such a capacity fading is generally observed for anatase TiO_2. This behavior is not observed for the mesoporous compound. Hence, after 20 cycles at 2*C* rate the capacity retention is 96% (158 mAh g^{-1}) and 100% (130 mAh g^{-1}) using 1.2–3 and 1.5–3 V potential ranges.

The specific charge discharge capacity of TiO_{2meso} at different *C* rates was also studied (Fig. 5). The specific capacity shows excellent values for charging rates up to 2*C* for both studied potential windows. Indeed, the measured specific capacities are about 158 and 127 mAh g^{-1} at 2*C* and 6*C*, respectively (potential window 1.2–3 V). For the potential window 1.5–3 V, the specific capacity is 129 mAh g^{-1} at 2*C* and 107 mAh g^{-1} at 6*C*. At low charging rate (*C*/5), capacity is 184 mAh g^{-1} for 1.2–3 V voltage window and 148 mAh g^{-1}. This latest value is inferior to maximal theoretical one (168 mAh g^{-1}) suggesting that TiO_{2meso} is not fully crystallized. Initial values of capacity are recovered after the slowest step with no capacity loss. Finally, TiO_{2meso} displays high capacities, excellent reversibility and stability upon cycling.

Besides its high capacity, TiO_{2meso} anatase electrodes also exhibit high rate performances. The capacity decreased steeply with increasing the charging rate suggesting that a polariza-

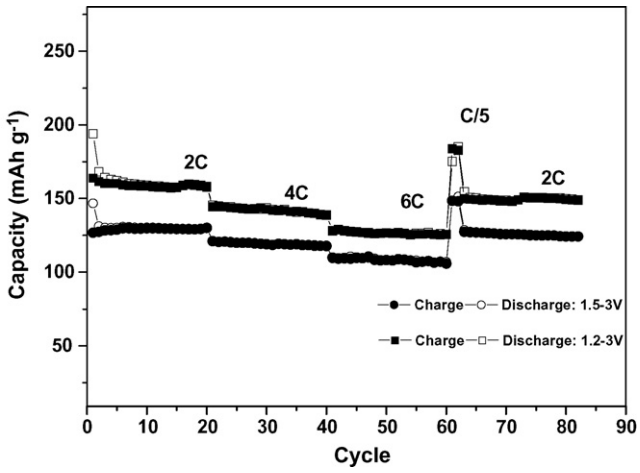

Fig. 5. Specific charge/discharge capacity of TiO_{2meso} using 1.5–3 and 1.2–3 V potential windows.

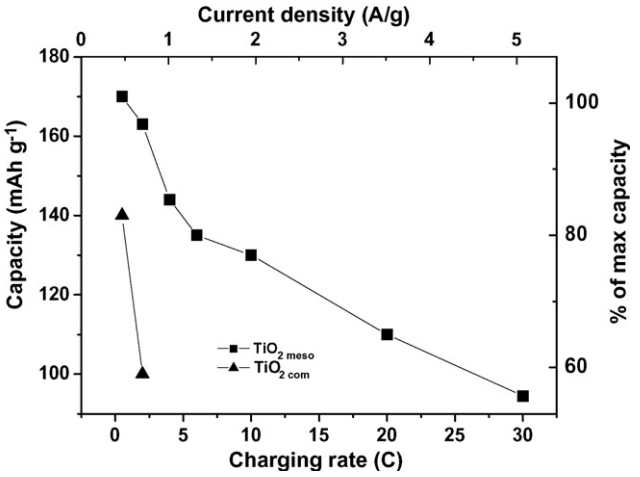

Fig. 7. Capacity of lithium insertion/extraction vs. charging rate for TiO_{2com} and TiO_{2meso}.

tion due to electrolyte resistance or electric resistance of TiO_2 increased with increasing the charging rate. Fig. 6 shows the potential–capacity profile of TiO_{2meso} at different current rates between 1.2 and 3 V. At the lowest rate (2*C*, 0.335 A g^{-1}), the plateau at 1.78 V is still present. It disappeared progressively with increasing the charging rate up till 30*C*. On the contrary, the plateau feature is conserved whatever the charging rate, the voltage plateau is about 2.2 V at 30*C* rate. This behavior suggests that the insertion step is the more limiting parameter. Fig. 7 presents the current density dependence of the charge (extraction) capacities of TiO_{2meso} and TiO_{2com}. The specific charge capacity of TiO_{2meso} remains 130, 110 and 95 mAh g^{-1} at 10*C* (1.68 A g^{-1}), 20*C* (3.35 A g^{-1}) and 30*C* (5.04 A g^{-1}) corresponding to 0.39, 0.33 and 0.28 reversible Li per mole of TiO_2 while the capacity of TiO_{2com} drops quickly from 140 mAh g^{-1} at *C*/5 to 98 mAh g^{-1} at 2*C* rate. Such high rate capability has been recently reported [44,45] for anatase TiO_2. In addition, our material displays lower apparent surface area (92 m^2 g^{-1}) than previously reported values. It suggests that large surface area is not the key point for good electrochemical performances. The presence of mesopores is also important for high rate performances and favorable for electrolyte ions transport.

3.2.3. Deinsertion capabilities

Kavan et al. reported that mesoporosity in TiO_2 leads to unusual properties in the charging regime [9]. In order to evaluate these properties the charging abilities of TiO_{2meso} has been investigated using slow discharge (*C*/5) and fast charge (2*C* and 4*C*) rates. The corresponding galvanostatic insertion/extraction curve is shown in Fig. 8. It exhibits a well-defined plateau at 1.78 V during discharge and plateaus at 1.99 V (charge 2*C*) and 2.07 V (charge 4*C*). The specific charge capacities are 165 and 156 mAh g^{-1} at 2 and 4*C* for charge with almost 100% of reversibility. These values are close to the theoretical one which (168 mAh g^{-1}) and higher than those observed using the same rate for charge and discharge.

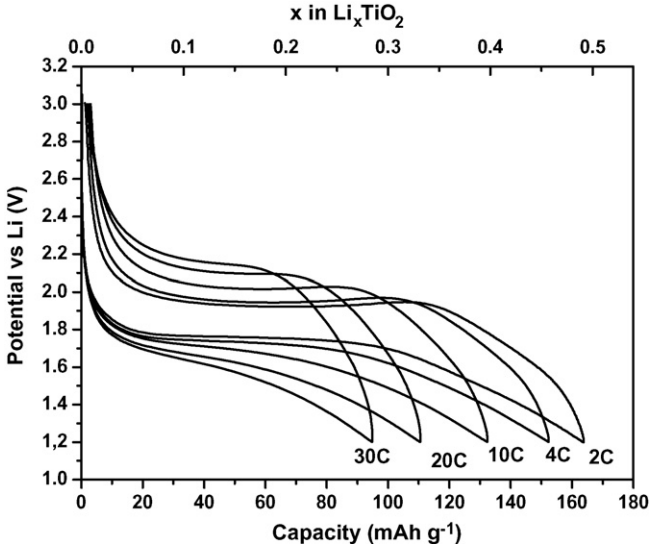

Fig. 6. Typical galvanostatic Li^+ insertion/extraction curves into mesoporous TiO_2 at different charging rates from 2*C* to 30*C*.

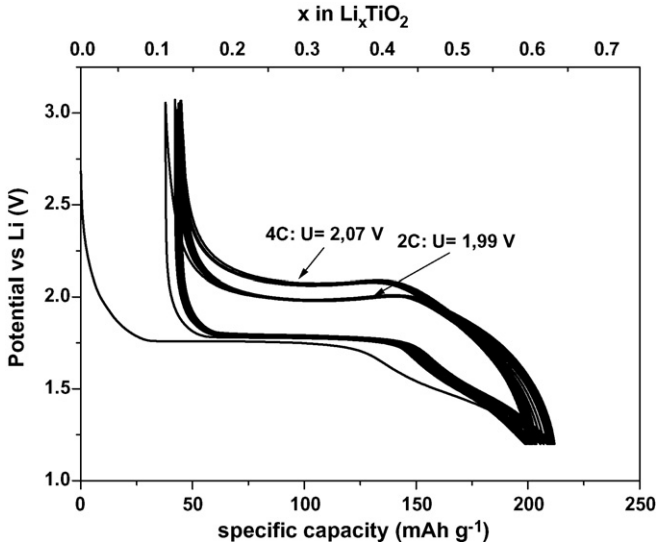

Fig. 8. Galvanostatic Li^+ insertion/extraction into mesoporous TiO_2 at constant charge current (*C*/10) and different discharge current 2*C* and 4*C*.

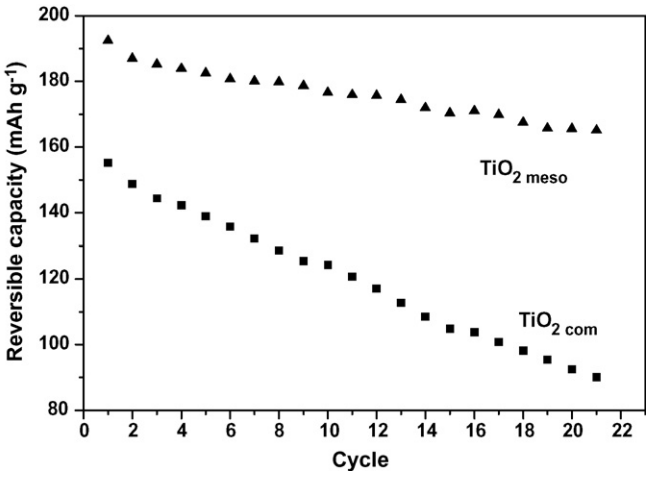

Fig. 9. Evolution of reversible capacity for both TiO_{2com} and TiO_{2meso}, applying currents $C/5$ in discharge current, and $2C$ in charge between 1.2 and 3 V potential window.

The same kind of experiment has been performed with commercial anatase in order to compare to the mesoporous material. The evolution of reversible capacity (Fig. 9) shows that mesoporous TiO_2 presents higher charging abilities than the commercial one. The capacity decreases rapidly for commercial TiO_2 while it remains stable for the mesoporous material. After 10 cycles, the measured capacity is 119 mAh g^{-1} for TiO_{2com} (76% of its first reversible capacity), only 4% loss of capacity is observed for TiO_{2meso}.

TiO_{2meso} displays also high deinsertion properties with almost 100% reversibility at extraction rates from $2C$ to $15C$. The observed reversible capacities are 151, 143 and 135 mAh g^{-1} at the charge currents $10C$ (1.68 A g^{-1}), $20C$ (3.35 A g^{-1}) and $30C$ (5 A g^{-1}). However, as can be seen in Fig. 10, we observe a strong increase in the voltage profile during the deinsertion process which can be due to electrolyte resistance. Although the exact role of mesopores is still unknown, it seems to favor

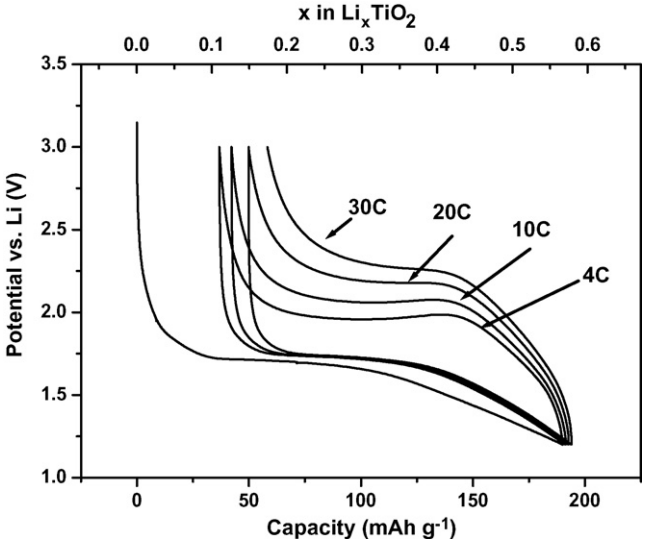

Fig. 10. Galvanostatic Li^+ insertion/extraction into mesoporous TiO_2 at constant discharge current $2C$ and different charge currents $4C$, $10C$, $20C$ and $30C$.

the lithium extraction from anatase TiO_2 and it leads to high capacities at relatively high rates.

4. Conclusion

The electrochemical lithium insertion into mesoporous anatase TiO_2 synthesized using an ethylene glycol-modified titanium-precursor and an amphiphilic molecule as the templating agent has been investigated. It shows high charging/discharging capabilities and remarkable stability. Moreover, it exhibits excellent extraction capabilities with capacities close to the theoretical value. Its electrochemical properties should be discussed not only in terms of surface area, crystallite size but also of mesopore size.

Acknowledgment

Financial support from DFG under SP1181 program is gratefully acknowledged.

References

[1] D. Murphy, R. Cava, S. Zahurak, A. Santoro, Solid State Ionics 9–10 (1983) 413.
[2] B. Zachau-Christiansen, K. West, T. Jacobsen, S. Atlung, Solid State Ionics 28–30 (1998) 1176.
[3] T. Ohzuku, T. Kodoma, T. Hirai, J. Power Sources 46 (1985) 61.
[4] S. Huang, L. Kavan, I. Exnar, M. Grätzel, J. Electrochem. Soc. 142 (1995) L142.
[5] L. Kavan, M. Grätzel, J. Rathousky, A. Zukal, J. Electrochem. Soc. 143 (1996) 394.
[6] G. Armstrong, R. Armstrong, J. Canales, R. Garcia, P. Bruce, Adv. Mater. 17 (2005) 862.
[7] G. Armstrong, R. Armstrong, P. Bruce, P. Reale, B. Scrosati, Adv. Mater. 18 (2006) 2597.
[8] L. Kavan, A. Attia, F. Lenzmann, S. Elder, M. Grätzel, J. Electrochem. Soc. 147 (2000) 2897.
[9] L. Kavan, J. Rathousky, M. Grätzel, V. Shklover, A. Zukal, J. Phys. Chem. B 104 (2000) 12012.
[10] L. Kavan, J. Prochazka, T. Spitler, M. Kalbac, M. Zukalova, T. Drezen, M. Grätzel, J. Electrochem. Soc. 150 (2003) A1000.
[11] C. Kresge, M. Leonowicz, W. Roth, J. Vartuli, J. Beck, Nature 359 (1992) 710.
[12] D. Antonelli, J. Ying, Angew. Chem. 107 (1995) 2202.
[13] P. Liu, J. Reddy, A. Adnot, A. Sayari, Mat. Res. Soc. Symp. Proc. 431 (1996) 101.
[14] P. Liu, J. Liu, A. Sayari, Chem. Commun. 6 (1997) 577.
[15] G. Pacheco, E. Zhao, A. Garcia, A. Sklyarov, J. Fripiat, J. Mater. Chem. 8 (1998) 219.
[16] A. Stein, M. Fendorf, T. Jarvie, K. Mueller, M. Garcia, T. Mallouk, Mat. Res. Soc. Symp. Proc. 371 (1995) 69.
[17] V. Stone, R. Davis, Chem. Mater. 10 (1998) 1468.
[18] A. Fujishima, K. Honda, Nature 37 (1972) 238.
[19] L. Kavan, J. Rathousky, M. Grätzel, V. Shklover, A. Zukal, Microporous Mesoporous Mater. 44-45 (2001) 663.
[20] I. Moriguchi, R. Hidaka, H. Yamada, T. Kudo, Solid State Ionics. 176 (2005) 2361.
[21] H. Zhou, D. Li, M. Hibino, I. Honma, Angew. Chem. Int. Ed. 44 (2005) 797.
[22] D. Fattakhova, M. Wark, T. Brezesinski, B. Smarsly, J. Rathousky, Adv. Funct. Mater. 17 (2007) 123.
[23] L. Kavan, A. Attia, F. Lenzmann, S. Elder, M. Grätzel, J. Electrochem. Soc. 147 (8) (2000) 2897.

[24] A. Attia, M. Zukalova, J. Rathousky, A. Zukal, L. Kavan, J. Solid State Electrochem. 9 (2005) 138.
[25] Z. Peng, Z. Shi, M. Liu, Chem. Commun. 21 (2000) 2125.
[26] S. Hartmann, D. Brandhuber, N. Hüsing, Acc. Chem. Res. 40 (2007) 885.
[27] X. Jiang, T. Herricks, Y. Xia, Adv. Mater. 15 (2003) 1206.
[28] M. Pal, J. Serrano, P. Santiago, U. Pal, J. Phys. Chem. C 111 (2007) 96.
[29] M. Fröba, H. Thoms, M. Epple, J. Wong, A. Reller, J. Mater. Chem. 8 (1998) 1447.
[30] Y. Xia, J. Xuchuan, T. Herricks, Adv. Mater. 15 (2003) 1205.
[31] G. Sudant, E. Baudrin, D. Larcher, J.M. Tarascon, J. Mater. Chem. 15 (2005) 1263.
[32] S. Brunauer, P. Emmett, E. Teller, J. Am. Chem. Soc. 60 (1938) 309.
[33] R. Van de Krol, A. Goossens, E. Meulenkamp, J. Electrochem. Soc. 146 (1999) 3150.
[34] R. Hengerer, L. Kavan, P. Krtil, M. Grätzel, J. Electrochem. Soc. 147 (2000) 1467.
[35] M. Wagemaker, A. Kentgens, F. Mulder, Nature 418 (2002) 397.
[36] P. Krtil, L. Kavan, D. Fattakhova, J. Solid State Electrochem. 1 (1997) 83.
[37] P. Krtil, D. Fattakhova, L. Kavan, S. Burnside, M. Grätzel, Solid State Ionics 135 (2000) 101.
[38] D. Fattakhova, L. Kavan, P. Krtil, J. Solid State Electrochem. 5 (2001) 196.
[39] L. Kavan, M. Kalbac, M. Zukalova, I. Exnar, V. Lorenzen, R. Nesper, R. Grätzel, Chem. Mater. 16 (2004) 477.
[40] X. Gao, H. Zhu, G. Pan, S. Ye, Y. Lan, F. Wu, D. Song, J. Phys. Chem. B 108 (2004) 2868.
[41] L. Aldon, P. Kubiak, A. Picard, J.C. Jumas, J. Olivier-Fourcade, Chem. Mater. 18 (2006) 1401.
[42] M. Smirnov, R. Baddour-Hadjean, J. Phys. Chem. 121 (2004) 2348.
[43] R. Baddour-Hadjean, S. Bach, M. Smirnov, J.P. Pereira-Ramos, J. Raman Spectrosc. 35 (2004) 577.
[44] I. Moriguchi, R. Hidaka, H. Yamada, T. Kudo, H. Muratami, N. Nakashima, Adv. Mater. 18 (2006) 69.
[45] C. Jiang, M. Wei, Z. Qi, T. Kudo, I. Honma, H. Zhou, J. Power Sources 166 (2007) 239.